SANDIA REPORT
SAND2013-8035
Unlimited Release
Printed September 2013

Fielding the Magnetically Applied Pressure-Shear Technique on the Z Accelerator (completion report for MRT 4519)

C. Scott Alexander, Thomas A. Haill, Devon G. Dalton, Dean C. Rovang, Derek C. Lamppa

Prepared by
Sandia National Laboratories
Albuquerque, New Mexico 87185 and Livermore, California 94550

Sandia National Laboratories is a multi-program laboratory managed and operated by Sandia Corporation, a wholly owned subsidiary of Lockheed Martin Corporation, for the U.S. Department of Energy's National Nuclear Security Administration under contract DE-AC04-94AL85000.

Issued by Sandia National Laboratories, operated for the United States Department of Energy by Sandia Corporation.

Available to DOE and DOE contractors from
U.S. Department of Energy
Office of Scientific and Technical Information
P.O. Box 62
Oak Ridge, TN 37831

Telephone: (865) 576-8401
Facsimile: (865) 576-5728
E-Mail: reports@adonis.osti.gov
Online ordering: http://www.osti.gov/bridge

Available to the public from
U.S. Department of Commerce
National Technical Information Service
5285 Port Royal Rd.
Springfield, VA 22161

Telephone: (800) 553-6847
Facsimile: (703) 605-6900
E-Mail: orders@ntis.fedworld.gov
Online order: http://www.ntis.gov/help/ordermethods.asp?loc=7-4-0#online

SAND2013-8035
Unlimited Release
Printed September 2013

Fielding the Magnetically Applied Pressure-Shear Technique on the Z Accelerator (completion report for MRT 4519)

C. Scott Alexander, Thomas A. Haill, Devon G. Dalton, Dean C. Rovang, Derek C. Lamppa

Sandia National Laboratories
P.O. Box 5800
Albuquerque, New Mexico 87185

Abstract

The recently developed Magnetically Applied Pressure-Shear (MAPS) experimental technique to measure material shear strength at high pressures on magneto-hydrodynamic (MHD) drive pulsed power platforms was fielded on August 16, 2013 on shot Z2544 utilizing hardware set A0283A. Several technical and engineering challenges were overcome in the process leading to the attempt to measure the dynamic strength of NNSA Ta at 50 GPa. The MAPS technique relies on the ability to apply an external magnetic field properly aligned and time correlated with the MHD pulse. The load design had to be modified to accommodate the external field coils and additional support was required to manage stresses from the pulsed magnets. Further, this represents the first time transverse velocity interferometry has been applied to diagnose a shot at Z. All subsystems performed well with only minor issues related to the new feed design which can be easily addressed by modifying the current pulse shape. Despite the success of each new component, the experiment failed to measure strength in the samples due to spallation failure, most likely in the diamond anvils. To address this issue, hydrocode simulations are being used to evaluate a modified design using LiF windows to minimize tension in the diamond and prevent spall. Another option to eliminate the diamond material from the experiment is also being investigated.

ACKNOWLEDGEMENTS

The authors wish to recognize the contributions of many individuals who supported this effort on Z. The entire Z operations staff who did a wonderful job of preparing the machine to fire in a new configuration; especially the center section staff who installed much of the new hardware. The STAR and DICE staff who graciously loaned hardware necessary for the transverse velocimetry without which the experiment would not have been possible. Especially Randy Hickman who assisted in the fielding of the loaded hardware at Z and Nicole Cofer who built the targets. Dan Dolan who fielded a secondary PDV diagnostic during the shot. Finally, Anthony Romero, Charlie Meyer, and Jeff Gluth who fabricated hardware for and fielded the primary velocimetry system.

CONTENTS

Contents

INTRODUCTION

Shear strength is defined as the ability of a material to support deviatoric stress. While strength is an important material property affecting the outcome of many dynamic materials problems, the measurement of strength is not trivial at high pressures and strain rates. Several techniques have been employed over the past several decades; each with their own limitations. Oblique impact [1] and lateral stress gauge [2] techniques are limited to very low pressures (under 20 GPa). Stress difference between shock and isentropic loading [3] leads to large uncertainties. Rayleigh-Taylor instability growth [4] requires strength models be known in order to analyze the data making the testing more suitable to validation. Wave profile techniques exploiting the quasi-elastic release from a peak compression state [5] currently offer the best precision at high pressures but still require assumptions be made about the nature of the release and are prone to other uncertainties due to the range of pressures over which the release occurs. For these reasons, a new approach to strength measurement was developed at Sandia National Laboratories to directly measure dynamic material strength. The resultant method, known as magnetically applied pressure-shear (MAPS) [6], allows for a direct measure of strength absent the assumptions and complications associated with the other common approaches.

MAPS principles of operation

MAPS experiments on Z are based on a coaxial load MHD drive platform utilized for many dynamic material properties experiments as illustrated in figure 1a. The energy from the accelerator is used to drive a current along the cathode and anode faces (black arrows). This current flows in a loop inducing a magnetic field (blue vectors, in and out of page) within the A-K gap. The interaction of current and magnetic field results in a Lorentz force (blue arrows) which acts outward on the drive panels creating a pressure wave.

In the MAPS configuration, illustrated in figure 1b, pulsed magnetic field coils are added to apply an external magnetic field (red arrows). A Lorentz force results from the interaction of the external field and the drive current creating a shear force (yellow vectors, in and out of page) in both the anode and cathode. In the anode material, the shear force creates a shear wave in addition to the longitudinal compression wave.

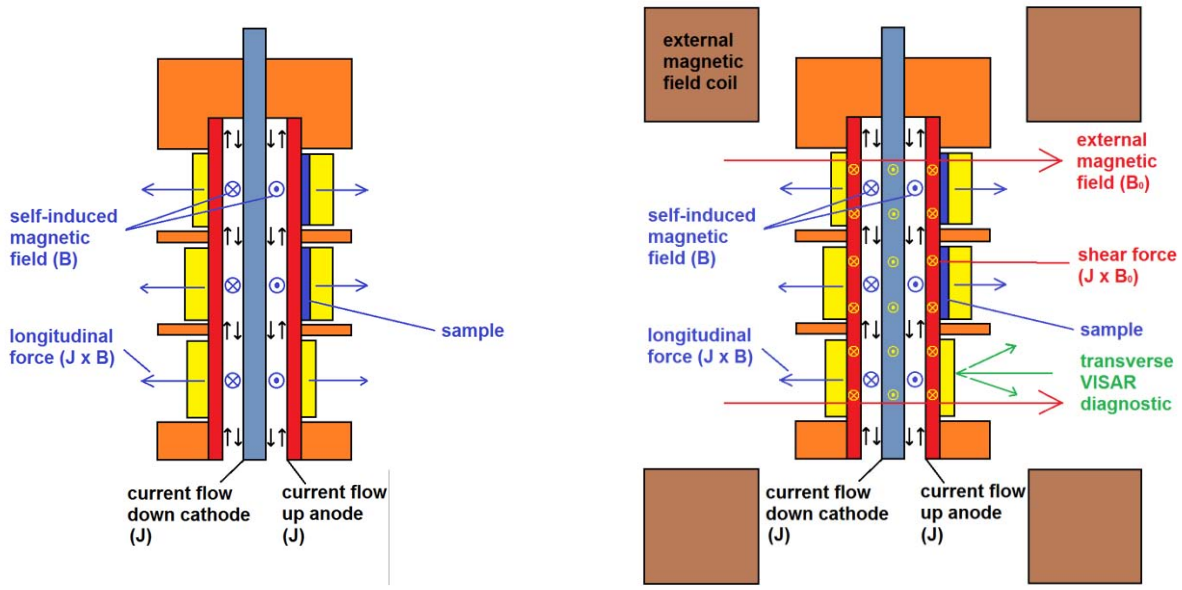

(a) (b)

Figure 1: Illustration (a) of a standard coaxial load design and (b) a MAPS configuration.

Wave propagation during a MAPS experiment is critical to determining the dynamic strength of the sample material. Figure 2 illustrates a typical MAPS experiment. There are three material layers present. The driver is the anode material described above where both the longitudinal and shear waves are generated. Note that the shear wave travels at a lower speed and trails behind the longitudinal wave. The experiment is designed such that the shear wave will travel faster than the magnetic diffusion front, the location where the self-induced magnetic field has diffused into the driver and typically associated with a very high temperature plasma state and associated loss of strength. Both waves, longitudinal and shear, travel to the right. Bonded to the driver is the sample layer. Upon arrival of the longitudinal wave, the sample is compressed to a high pressure state determined by both the magnitude of the wave and also the driver and sample equations of state (EOS). After the sample is fully compressed to peak pressure, the arrival of the shear wave probes the sample strength. The driver material is selected such that it will support more shear than the sample. In addition, the experiment is designed so that more shear is generated in the driver than the sample can support. Thus, upon arrival of the shear wave at the sample, the magnitude of the shear wave is truncated to the maximum supported shear in the sample; that is the sample strength. This is illustrated in figure 2 by the dotted yellow lines showing the shear wave magnitude. As the waves continue to propagate, they reach the anvil. The purpose of the anvil layer is to prevent a release wave from forming when the longitudinal wave reaches the back of the sample. Instead, the longitudinal wave is allowed to propagate into the anvil delaying release until the wave reaches the free surface at the back side. This allows sufficient time for the shear waves to fully exit the sample. Another important design consideration is that the anvil must be capable of supporting the full shear stress present in the sample to prevent further truncation of the shear wave at the sample-anvil interface. Upon arrival at the free surface, both wave magnitudes are measured via velocity interferometry. The longitudinal and shear stresses can be calculated directly from the velocity data.

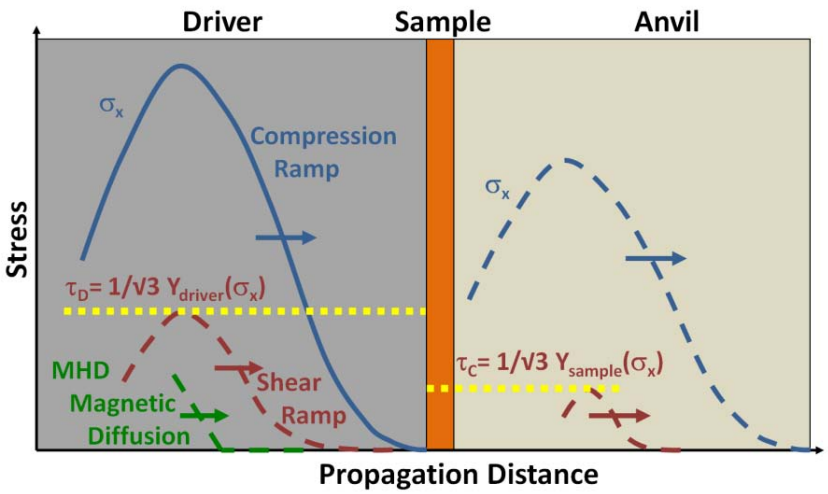

Figure 2: Wave propagation during a MAPS experiment.

A specialized velocity interferometer system for any reflector (VISAR), similar to that used by Chhabildas and Swegle [7], is used to measure both longitudinal and transverse velocities at the anvil free surface. Normally incident light is collected at nominally 17° and 25° off-axis and analyzed to determine both longitudinal and transverse particle velocities.

Strength is determined directly from the results of the experiment. The peak longitudinal velocity is analyzed to determine the peak compression of the sample. The peak transverse velocity is then directly related to the shear stress transmitted by the sample and hence gives the strength. In order to perform both analyses, the only required data are the peak velocities and the properties of the anvil material (density, acoustic wave velocity).

Previous work

The MAPS technique has been proven on the smaller scale Sandia Veloce machine. Initial testing on aluminum at about 9 GPa was reported previously [6]. The results are shown in figure 3a. Additional low pressure testing on tantalum was conducted as part of the preparatory work for implementation on Z. Results of that test are shown in figure 3b.

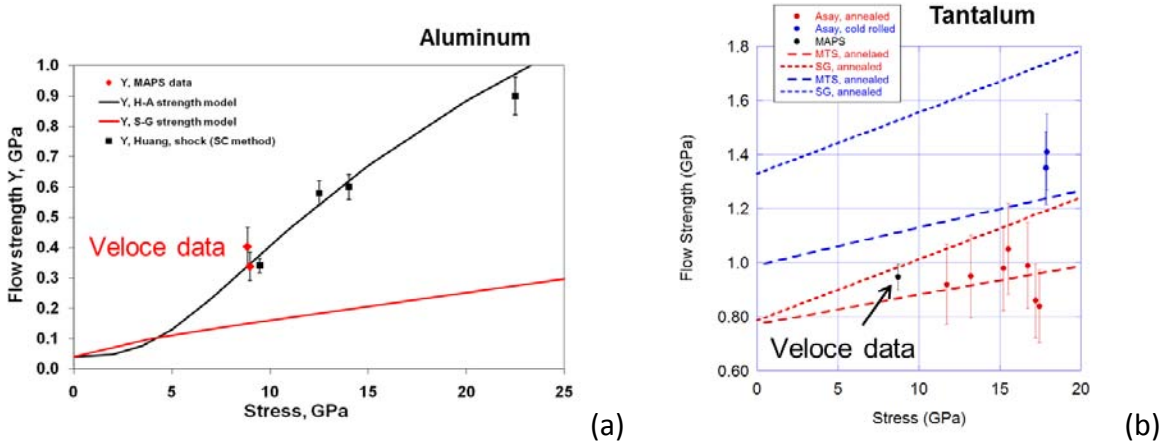

Figure 3: Results of previous MAPS strength testing.

In both figures, additional data collected by other techniques[8-10] is shown for comparison along with relevant strength models [11, 12] (curves). In all cases, the MAPS data was consistent with existing data and, more importantly, was sufficiently well defined as to discriminate between the various proposed strength models. In the case of Ta, existing data could not discriminate well in the case of annealed Ta (red points).

IMPLEMENTATION ON Z

In order to conduct these experiments on Z [13], the hardware framework established on Veloce [14] was required to be transitioned to the Z platform. As Veloce and Z operate under similar principles, this was mostly a problem of adapting to the different geometry.

External Magnetic Field Coils

The primary difference between a MAPS experiment and a standard isentropic compression shot is the requirement for an external magnetic field. In order to generate the field, a pair of pulsed Helmholtz coils are placed on opposite sides of the Z load. The coils are oriented such that the field generated will be normal to the plane of current flow in the driver in order to generate a shear loading. The coils used and the associated capacitive power supply were designed and constructed for joint use between the MAG-LIF and MAPS experimental programs [15].

When energized, the coils produce a magnetic field with a relatively long duration of approximately 4.75 ms (FWHM). This allows the field to be considered as static over the typical 1 μs duration of the Z experiment. In addition, the field produced is sufficiently spatially uniform. The field varies about 1.2% across the sample diameter.

Load Design

While the Veloce tests were conducted using a stripline geometry, it was decided to use a coaxial load design on Z. The coaxial design allows for the containment of the self-generated magnetic field within the load and preventing the need for additional shielding on the diagnostics. In addition, a coaxial load is better suited for the compression levels required for this test on Z. The use of a stripline load would make the pulse shape design much more challenging.

In order to achieve the field uniformity at the sample locations, the coils must be centered on the middle sample. This was not possible with the standard Z coaxial load design as the coils would interfere with the Z current feeds. To solve this problem, an extended coaxial load was designed. This elevated the samples from the anode plate to allow for clearance of the coils. The extended design used with a bell jar style feed would result in a significant increase in load inductance. Predictive calculations of machine performance critical to implementing the desired pulse shape are less reliable with increased load inductance. As a result, the feed was redesigned with a radial feed gap which reduced the inductance gain over a standard design to within acceptable limits.

The final consideration in adapting the field coils for used on Z was mitigation of the stress resulting from pulsing the coils. When the coils are energized, axial loads of approximately 30,

000 pounds are generated between the two coils. Forces are much smaller in the off-axial directions but still must be managed. In order to support the coils such that there is little to no motion of both the coils and the Z load while being energized, a support structure was designed into the load. Figure 4 shows the central portion of a Z load with the external field coils in place. The central support structure protects the coaxial load while the large superstructure manages the repulsive axial load as well as the smaller off-axis loads. Testing performed at the Systems Integration Test Facility prior to use on Z indicated no issues with coil or load motion during the coil firing sequence.

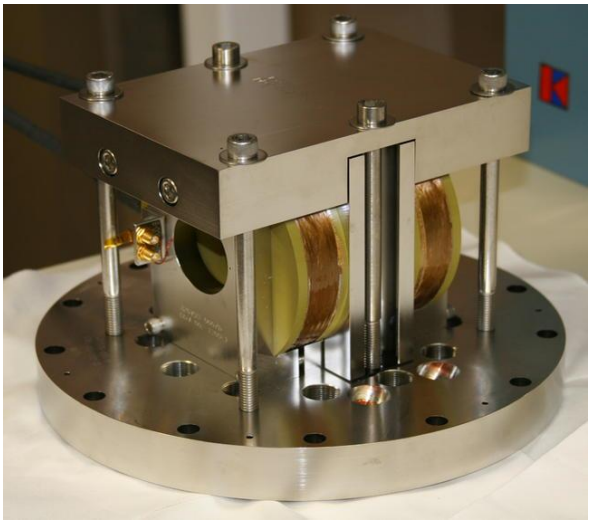

Figure 4: External field coils shown with the supporting superstructure on a Z load.

EXPERIMENTAL DESIGN

The materials selected for the Z experiment were determined based on the selection criteria outlined earlier. Molybdenum was selected as the driver material based on its high strength and good electrical conductivity (required for Z to function properly). Tantalum was selected as the sample material due to programmatic importance and also because of the large existing strength data set to compare the results with. Polycrystalline diamond was selected for the anvil material based on the previously detailed constraints and the desire to prevent any plastic deformation in the anvil during the experiment. This constraint greatly simplifies the data analysis. The use of diamond anvils was the only substantial change from the previous Veloce test.

All aspects of the MAPS experiment (driver, sample, and anvil dimensions; current pulse shape) were designed using the ALEGRA hydrocode [16]. A 2D Cartesian geometry with an Eulerian mesh (5-10 micron cells) was used and is illustrated in figure 5. Periodic boundary conditions were applied in the transverse (Y) direction. The external magnetic field was imposed as a static field in the simulations as this is a good approximation to the experiment given the wide discrepancy in time scales associated with the pulsed field compared with the Z experiment. The simulations were driven with a tangent magnetic field derived from a desired drive current pulse shape. Models used are detailed in table I. Results of the simulations are output at the tracer locations indicated by the black dots in figure 5. These will be identified as the driver, sample, anvil, and free surface.

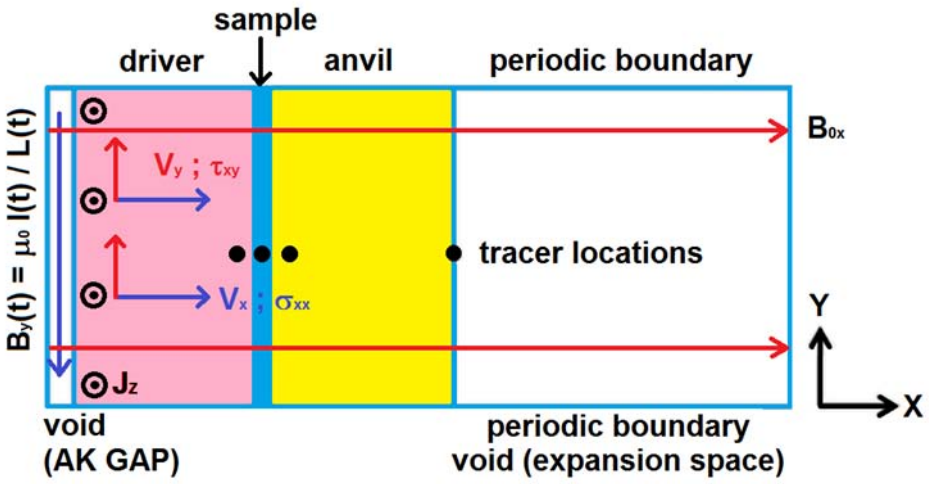

Figure 5: ALEGRA computational domain for all design simulations. Black dots show tracer locations.

Table I: Model parameters used in the ALEGRA simulations.

MAPS Materials and Material Model Parameters							
Panel Layer Material	Equation of State	Strength Model	Conductivity Model	Density (g/cm^3)	Longitudinal Wave Speed (km/s)	Shear Wave Speed (km/s)	Yield Strength (GPa)
Driver Molybdenum	LANL Sesame 2984	CTH Elastic-Plastic Steinberg-Guinan-Lund	Lee-More-Desjarlais (LMD)	10.22	6.45-6.45	3.47-3.48	0.9
Sample Tantalum	LANL Sesame 3720	CTH Elastic-Plastic Steinberg-Guinan-Lund	Lee-More-Desjarlais (LMD)	16.654	3.35-4.16	2.07-2.09	0.375
Anvil Diamond	LANL Sesame 7834	CTH Elastic Perfectly Plastic	Insulator	3.5126	18.328	11.659-12.0	50-90

The current pulse shape to be used on Z was designed such that the strength of the sample is probed as close as possible to the maximum compression. This is achieved by varying the drive pulse such that the longitudinal wave provides a region of near steady compression and the shear wave traverses the sample during this region. The final result is illustrated in figure 6 where we make use of a coupling relationship first noted by Swegle and Chhabildas [17] that states:

$$\frac{3}{4}\tau_{xx}^2 + \tau_{xy}^2 \le \frac{1}{3}\left(Y(P)\right)^2 \qquad (1)$$

where τ_{xx} is the longitudinal deviatoric stress, τ_{xy} is the shear stress, and Y is the strength. From the figure, it is clear that the probing shear wave (τ_{xy}) is a maximum near the peak of the longitudinal compression (proportional to Y). Further, at this point, shear stress is equal to the strength and the longitudinal deviatoric stress (τ_{xx}) is seen to be zero hence the equality in equation 1 holds. This is critical as equality is required for the strength to be calculated from the transmitted shear wave.

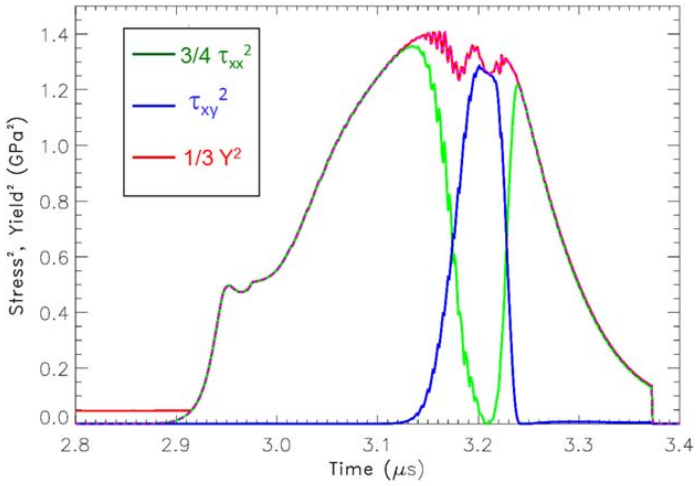

Figure 6: Stresses present in the sample using the optimized pulse shape along with the modeled sample strength.

Using the optimized pulse shape, the stresses present in all three materials are shown in figure 7. From the left plot, longitudinal compression of the sample is predicted to be 52.6 GPa maximum. The slight differences in longitudinal stress for each layer are due to impedance mismatch. On the right, it is seen that approximately 1.4 GPa shear stress is generated in the driver. Upon transmission to the weaker sample layer, the shear wave is truncated to a maximum of about 1.1 GPa. This truncated wave is seen to be fully supported in the anvil layer and hence the transverse velocities measured at the anvil free surface will be representative of the strength of the sample.

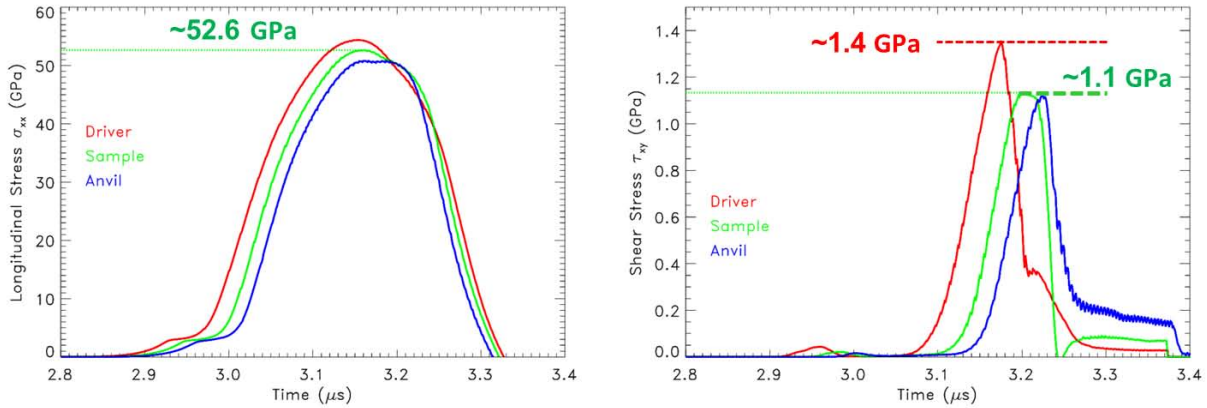

Figure 7: Simulated longitudinal and shear stresses in all three material layers using the optimized pulse shape and a 10 T static external magnetic field.

The predicted particle velocities are shown in figure 8. As shown, the driver, sample and anvil velocities are in situ while the free surface velocity is that predicted to be observed at the surface of the anvil. The free surface results predict the experimental data that will be collected during the experiment. Note that the longitudinal velocities are much higher (~1 km/s) than the transverse velocities (~0.01 km/s).

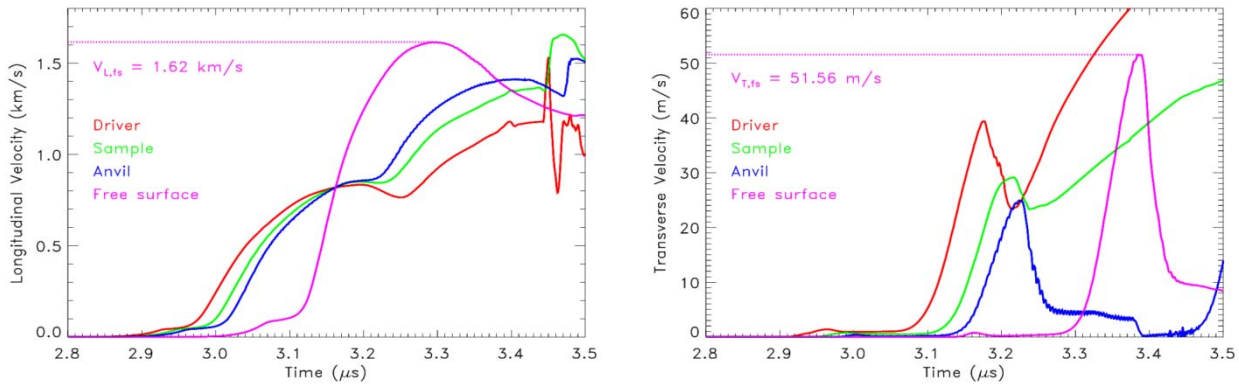

Figure 8: Predicted velocities for each layer and at the free surface of the anvil.

In order to provide a means for ensuring shear truncation at the sample, a control experiment is conducted omitting the sample layer. By omitting the sample, the full shear stress generated in the driver is transmitted to the anvil and detected at the free surface. In practice, the control experiment is fielded on an opposing panel to ensure as closely as possible identical loading of both the test sample and the control experiment. The effect can be seen in figure 7 where the full 1.4 GPa shear stress in the driver will be transmitted to the anvil when the sample is omitted. By conducting the experiment in this way, it can be ensured that truncation is observed.

EXPERIMENTAL RESULTS

Shot Z2544 was completed on August 16, 2013 utilizing hardware set A0283A. The shot was configured as illustrated in figure 9 with three samples on each side of the coaxial load. These are designated as locations 1, 3, and 5 from top to bottom. Thus, the top sample on the north facing panel is designated as N1. The bottom sample on the south panel is S5. Each of these samples is diagnosed with transverse capable VISAR. In addition, two normal VISAR diagnostics were fielded on each panel intermediate to the sample locations. These probes measure the motion of the Mo driver. This data will be used to develop unfold capability with molybdenum drivers in order to determine the drive current.

As illustrated in the figure and detailed in table II, sample locations S1 and S3 have Ta samples present backed with diamond anvils. The remaining four sample locations have only diamond anvils. These locations provide a check on the shear truncation as described previously in locations N1 and N3. The diamonds in locations N5 and S5 are designed to measure the longitudinal and shear velocities in the diamond. As will be shown, the determination of strength from the results requires knowledge of the longitudinal and shear wave speeds in the anvil material. By using two different thickness anvils in opposing sample locations, Lagrangian analysis can be used to determine the wave speeds.

Table II: Part dimensions for Z2544

Sample Location (see figure 9)	Mo Thickness (mm)	Ta Thickness (mm)	Diamond Thickness (mm)
N1	1.058	0	1.531
S1	1.033	0.119	1.898
N2	1.058	0	0
S2	1.033	0	0
N3	1.058	0	2.029
S3	1.033	0.010	2.005
N4	1.058	0	0
S4	1.033	0	0
N5	1.058	0	1.949
S5	1.033	0	1.539

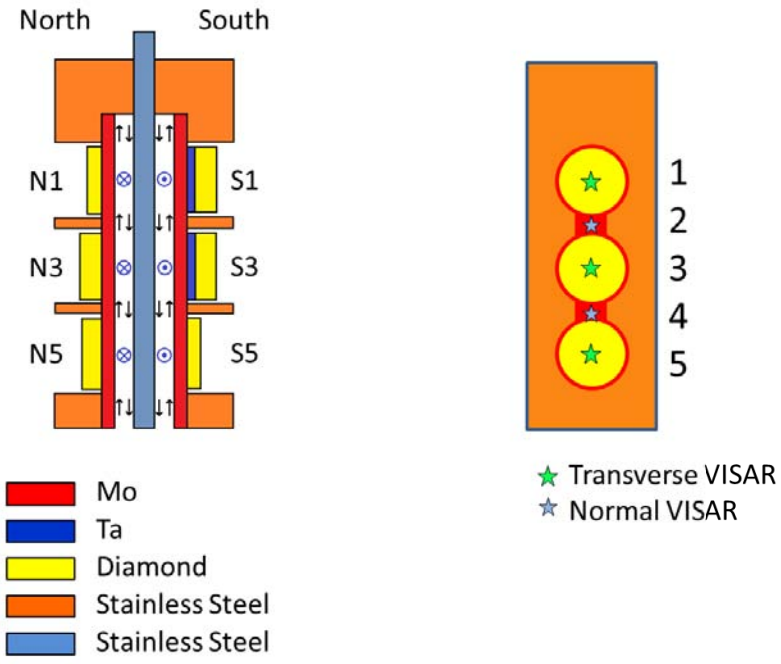

Figure 9: Illustration of sample locations for Z2544

Figure 10 shows representative velocity profiles as recorded by the 17 and 23 degree off-axis probes on sample N3; a 2 mm thick diamond anvil mounted to the Mo driver. All of the MAPS samples (locations 1, 3, and 5) are similar. In order to obtain useful information, the data is combined to determine both the longitudinal and transverse velocity profiles. These are shown in figure 11 for sample N3. Also shown in the figure are the predictions from figure 8. There are several discrepancies between the prediction and the data. Considering only the longitudinal velocity profiles for now, first, there is a variation in the timing of the main ramp loading with the experiment coming in about 30 ns early. This is likely due to machine performance differing from the predictive calculations and is not of concern to this experiment. Second, the peak longitudinal velocity is about 200 m/s lower than predicted. This could also be due to differences in machine performance but could also be due to current losses in the load. This load

design uses an elliptical feed design similar to previously used radial feeds which are known to result in current loss at the load. Regardless of the origin, the reduced peak velocity (corresponding to reduced peak pressure) is relatively minor and can be corrected in future shots by increasing the design current. Lastly, the recorded profile shows a plateau in the velocity just past the peak where the prediction shows a ramped release. This is particularly concerning as it indicates spall occurring in the anvil or a separation of the reflective coating from the anvil. As the longitudinal wave travels ahead of the transverse wave, if the anvil or reflector spall prior to detection of the shear wave, the data may be lost. However, looking now at the transverse data from figure 11, a sizeable transverse velocity is recorded. It is speculated that at least a portion of the shear wave had entered the spalled portion of the anvil prior to spallation. This portion of the wave was detected as transverse motion.

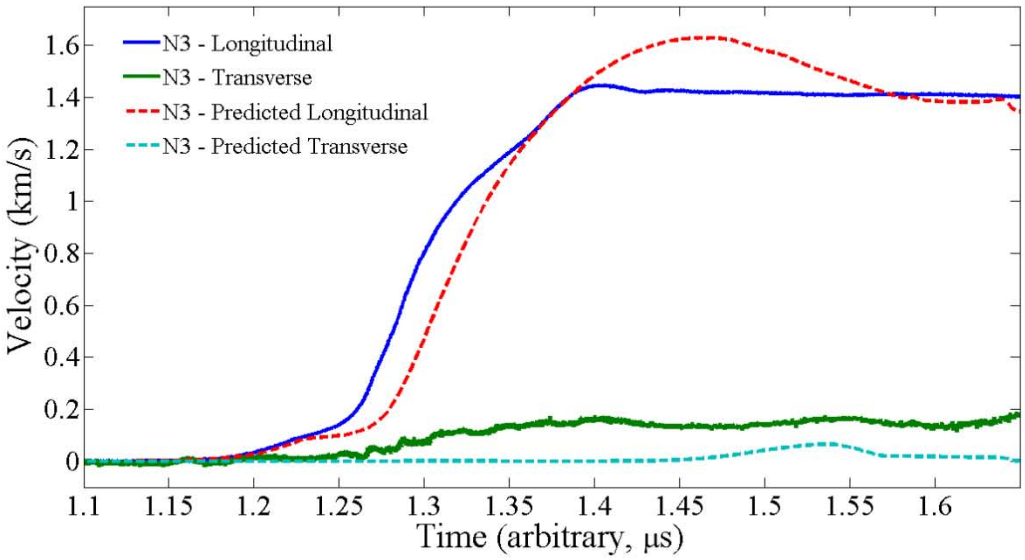

Figure 10: Longitudinal and transverse velocity profiles for sample location N3 compared with predicted values from ALEGRA simulations.

Similar data is shown in figure 11 for the S1 sample; a 0.1 mm Ta sample and a 2.0 mm diamond anvil mounted to the Mo driver. By comparison with figure 10, it is noted that very similar data was recorded regardless of the presence of the Ta sample in the S1 location. While this is not surprising for the longitudinal velocity as similar compression is expected, it is indicative of a failure of the strength experiment. As mentioned previously, MAPS relies on truncation of the shear wave by the sample. Similar transverse wave profiles indicate that no truncation was observed and hence any strength value determined would be a lower bound. This issue will be discussed further below when the data of figures 10 and 11 are directly compared.

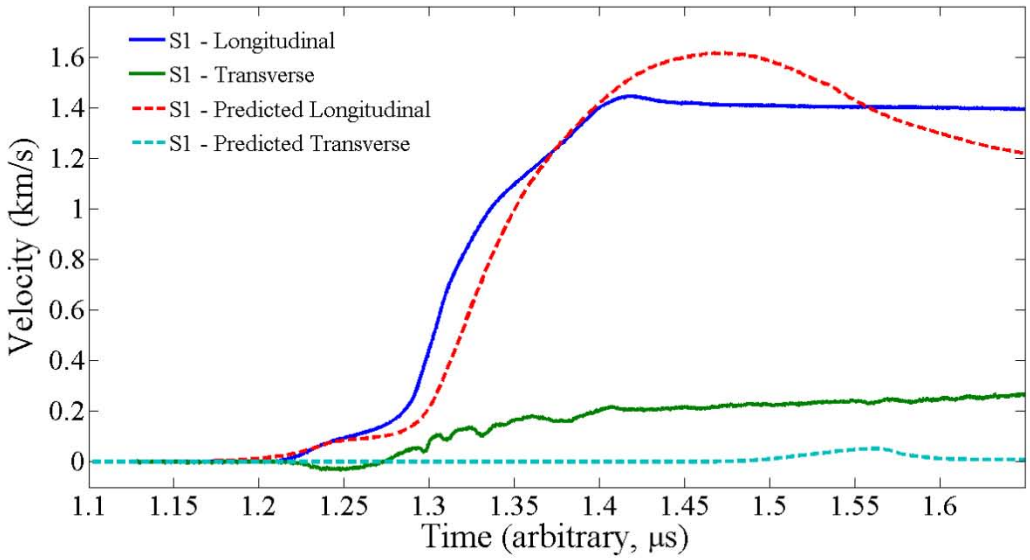

Figure 11: Longitudinal and transverse velocity profiles for sample location S1 compared with predicted values from ALEGRA simulations.

As noted previously, samples are compared on opposing locations to ensure similar loading profiles. In this case, the comparison is being performed between the north middle (N3) and south top (S1) locations. This is due to compromised data collected at the S3 location. Figure 12 shows a comparison of the data from S1 and S3; two nominally identical samples. As seen in the figure, the results are generally in agreement, however, there is a discrepancy in the S3 profile with a shock nearly forming during the elastic loading. This is not physically plausible as the samples above and below (S1 and S5) did not show such a response. In addition, the transverse data from S3 shows a wildly oscillatory response and drops out just past peak longitudinal compression; the time when spall likely occurred. For these reasons, it is believed that sample S1 provides a better basis for comparison with N3.

The S1 data can be directly compared with the N1 data. Figure 13 shows the data from N1, N3, and S1. Here it is clear that N1 and N3 show similar response with the only significant difference being in timing of the waves attributable primarily to the difference in anvil thickness on N1. Also, it can now be clearly seen that no truncation is observed in the shear wave passing through the Ta sample (S1). In fact, the shear wave passing through the Ta sample shows the greatest magnitude; although all are essentially equal within the experimental uncertainty of about +/- 10 m/s. This indicates that either insufficient shear was generated in the driver to probe the sample strength (full transmission, no truncation) or there was a loss of shear transmission due to spallation in the anvil. Based on the wave profiles indicating spallation occurring very shortly after peak compression, this is the most likely scenario.

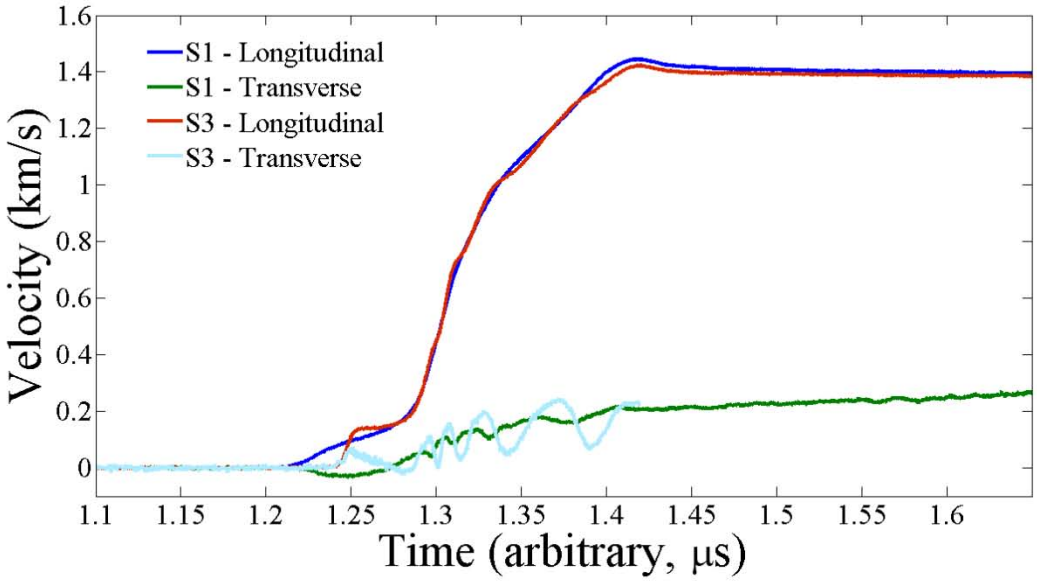

Figure 12: Comparison of the data from sample locations S1 and S3 indicate problems with the S3 data.

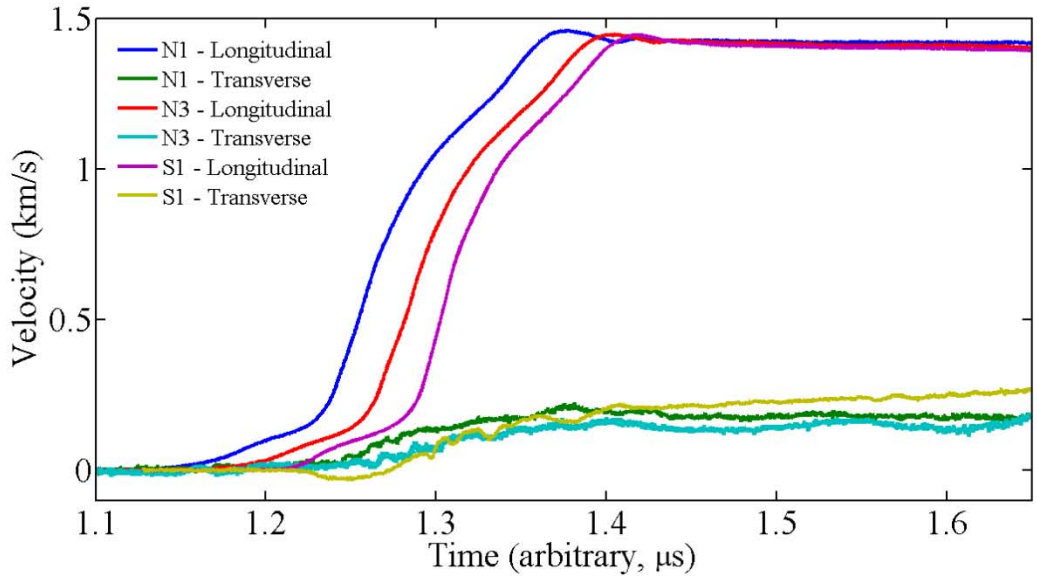

Figure 13: The data from sample locations N1, N3, and S1 are compared. Similar response is observed with differences being due to variations in driver, sample, and anvil thicknesses.

The velocity profiles for the samples in location 5, intended to be used to measure longitudinal and shear wave speeds in the diamond anvil material, are shown in figure 14. Similar to the MAPS samples, these also showed evidence of spallation. Further, there was evidence of reduced compression, perhaps due to the current loss issue on the south sample and increased noise in the transverse velocity. The combination of these issues prevented any analysis of this data pair.

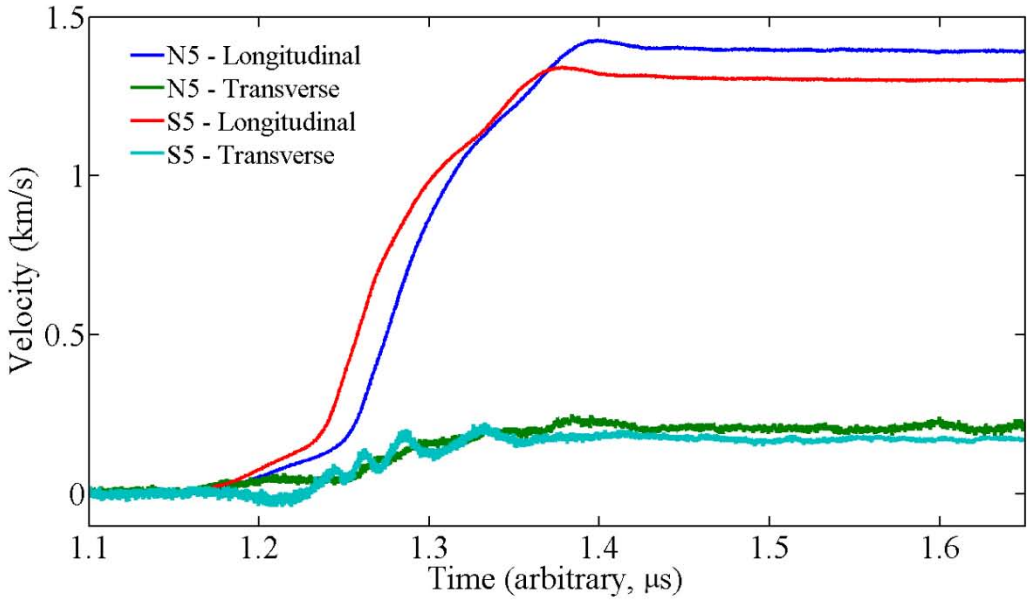

Figure 14: Velocity profiles for the samples in location 5 intended to measure the wave speeds in the diamond anvil material.

PATH FORWARD

The primary concern from shot Z2544 was the spallation which prevented acquisition of the full transverse velocity profile required for strength determination. As discussed above, all other issues can easily be addressed through modification of the design current pulse shape. Therefore, the path forward will focus on resolution of the spallation issue.

From the data, the spall most likely occurred in the diamond anvils. The diamond used is a polycrystalline diamond produced by a chemical vapor deposition (CVD) process. While this product has been tested and shown to have as good or better compressive strength than any other CVD diamond or even single crystal diamond tested, the spall strength has not been evaluated. If the CVD growth process results in particularly low spall strength, this could explain the experimental data. Spall strength of the diamond material can be further verified by additional testing using either Z or high velocity gas guns at Sandia's STAR facility. If the diamond spall strength is verified to be low, there are two options currently being investigated to remedy the problem and allow the MAPS shots to continue on Z.

Option 1 is to prevent spall in the diamond by reducing the magnitude of the tensile wave resulting from reflection of the longitudinal wave from the free surface. This can be accomplished by placing a LiF window on the back of the diamond. Impedance matching dictates that a portion of the longitudinal wave will be transmitted into the window and hence less will be reflected leading to reduced tension in the diamond. Numerical simulations using the ALEGRA hydrocode will be used to evaluate if a sufficient reduction in the tensile stress can be achieved. LiF is the only viable window option as it must remain transparent in order to measure the velocity profiles at the diamond-LiF interface.

Option 2 is to remove the diamond from the experiment. Replacing the diamond anvil with a LiF window will make the MAPS experiment much more complicated to analyze, but will ensure the issue of spall in the diamond is resolved. The main concern with this option is that due to the lower impedance of the LiF window, a significant release wave will propagate back into the sample as the longitudinal wave enters the window. This will significantly reduce the pressure at which the strength measurement is made as MAPS measure the minimum strength of the sample as the shear wave is transmitted. However, since the current experiments are near the lowest pressures achievable on Z, the peak compression can be increased in the design to account for the release wave. ALEGRA will again be used to evaluate the new design current pulse shape and verify that both the compression and shear can be measured in this configuration.

The current plan for the next MAPS experiment on Z is to use option 1. ALEGRA simulations are currently being conducted to verify the design. This option was selected as it will provide for the cleanest experiment with the lowest uncertainty and it does not require a redesign of the current pulse shape. In the future, option 2 will remain an active area of research as the removal of the diamonds from the experiment will result in significant cost savings.

SUMMARY

The MAPS technique to measure dynamic material strength was fielded on August 16, 2013 on shot Z2544 utilizing hardware set A0283A. The intent of the experiment was to measure the strength of NNSA Ta samples and compare the results to those obtained recently using other methods on Z. The shot utilized a current feed design and associated pulse shape, external pulsed magnetic field coils, and transverse capable VISAR diagnostics all of which had never been fielded on a dynamic materials Z shot prior to this attempt. All subsystems performed well with only minor issues related to the new feed design which can be easily addressed by modifying the current pulse shape. Unfortunately, despite the success of each new component, the experiment failed to measure strength in the samples due to spallation failure, most likely in the diamond anvils. To address this issue, hydrocode simulations are being used to evaluate a modified design using LiF windows to minimize tension in the diamond and prevent spall. Another option to eliminate the diamond material from the experiment is also being investigated.

REFERENCES

[1] A. S. Abousayed, R. J. Clifton and L. Hermann, 1976. Oblique-plate impact experiment, *Exp Mech* 16, p. 127-132.

[2] C. H. M. Simha and Y. M. Gupta, 2004. Time-dependent inelastic deformation of shocked soda-lime glass, *J. Appl. Phys.* 96, p. 1880-1890.

[3] G. R. Fowles, 1961. Shock wave compression of hardened and annealed 2024 aluminum, *J. Appl. Phys.* 32, p. 1475-1487.

[4] H. S. Park, K. T. Lorenz, R. M. Cavallo, S. M. Pollaine, S. T. Prisbrey, R. E. Rudd, R. C. Becker, J. V. Bernier and B. A. Remington, 2010. Viscous rayleigh-taylor instability experiments at high pressure and strain rate, *Physical Review Letters* 104, p. -.

[5] J. R. Asay and J. Lipkin, 1978. A self-consistent technique for estimating the dynamic yield strength of a shock-loaded material, *J. Appl. Phys.* 49, p. 4242-4247.

[6] C. S. Alexander, J. R. Asay and T. A. Haill, 2010. Magnetically applied pressure-shear: A new method for direct measurement of strength at high pressure, *J. Appl. Phys.* 108, p. 126101-126103.
[7] L. C. Chhabildas and J. W. Swegle, 1980. Dynamic pressure-shear loading of materials using anisotropic crystals, *J. Appl. Phys.* 51, p. 4799-4807.
[8] H. Huang and J. R. Asay, 2005. Compressive strength measurements in aluminum for shock compression over the stress range of 4-22 gpa, *J. Appl. Phys.* 98, p. 033524.
[9] H. Huang and J. R. Asay, 2007. Reshock and release response of aluminum single crystal, *J. Appl. Phys.* 101, p. 063550.
[10] J. R. Asay, T. Ao, T. J. Vogler, J. P. Davis and G. T. Gray, 2009. Yield strength of tantalum for shockless compression to 18 gpa, *J. Appl. Phys.* 106, p. 073515.
[11] D. J. Steinberg, S. G. Cochran and M. W. Guinan, 1980. A constitutive model for metals applicable at high-strain rate, *J. Appl. Phys.* 51, p. 1498-1504.
[12] S. R. Chen and G. T. Gray, 1996. Constitutive behavior of tantalum and tantalum-tungsten alloys, *Metallurgical and Materials Transactions A* 27, p. 2994-3006.
[13] C. A. Hall, J. R. Asay, M. D. Knudson, W. A. Stygar, R. B. Spielman, T. D. Pointon, D. B. Reisman, A. Toor and R. C. Cauble, 2001. Experimental configuration for isentropic compression of solids using pulsed magnetic loading, *Rev. Sci. Instrum.* 72, p. 3587-3595.
[14] T. Ao, J. R. Asay, S. Chantrenne, M. R. Baer and C. A. Hall, 2008. A compact strip-line pulsed power generator for isentropic compression experiments, *Rev. Sci. Instrum.* 79, p. 013903.
[15] D. Rovang, D. Lamppa, A. Owen, J. McKenney, D. Johnson, S. Radovich, C. S. Alexander, D. Dalton, T. Haill, M. Cuneo and D. Flicker, 2013, Completion memo of fy 2013 level-2 icf milestone mrt 4690: Commissioning of applied magnetic field capability on z for magnetically applied pressure shear (maps) experiments, A. N. M. Sandia National Laboratories
[16] A. C. Robinson, T. A. Brunner, S. Carroll, R. Drake, C. J. Garasi, T. Gardiner, T. Haill, H. Hanshaw, D. Hensinger, D. Labreche, R. W. Lemke, E. Love, C. Luchini, S. Mosso, J. Neiderhaus, C. Ober, S. Petney, W. J. Rider, G. Scovazzi, E. Strack, R. Summers, T. Trucano, G. Weirs, M. Wong and T. Voth, "ALEGRA: An Arbitrary Lagrangian-Eulerian Multimaterial, Multiphysics Code," AIAA 2008-1235, 46th AIAA Aerospace Science Meeting and Exhibit, Reno, NV (2008).
[17] J. W. Swegle and L. C. Chhabildas, in *Shock waves and high-strain-rate phenomena in metals*, edited by M. A. Meyers and L. E. Murr (Plenum Press, New York, 1981), pp. 401-415.

DISTRIBUTION

National Nuclear Security Administration
U.S. Department of Energy
Attn: Jason Pruet
Sherri Bingert
1000 Independence Ave., S.W.
Washington, DC 20585

MS 1169 Dept. 1600 J. R. Lee (electronic copy)
MS 1182 Dept. 5445 D.C. Lamppa (electronic copy)
MS 1189 Dept. 1641 T.A. Haill (electronic copy)
MS 1191 Dept. 1600 M.A. Sweeney (electronic copy)
MS 1193 Dept. 1688 D.C. Rovang (electronic copy)
MS 1195 Dept. 1640 D. G. Flicker (electronic copy)
MS 1195 Dept. 1646 C. S. Alexander (electronic copy)
MS 1195 Dept. 1646 J. L. Brown (electronic copy)
MS 1195 Dept. 1646 D.D. Dalton (electronic copy)
MS 1195 Dept. 1646 J-P. Davis (electronic copy)
MS 1195 Dept. 1646 D. H. Dolan III (electronic copy)
MS 1195 Dept. 1646 M. D. Furnish (electronic copy)
MS 1195 Dept. 1646 M. D. Knudson (electronic copy)
MS 1195 Dept. 1646 J. L. Wise (electronic copy)
MS 1195 Dept. 1647 G. Leifeste (electronic copy)
MS 9046 Dept. 8246 T. Vogler (electronic copy)
MS 0899 Dept. 9536 Technical Library (electronic copy)


Sandia National Laboratories